LANGMUIR Article
Cite This: *Langmuir* 2018, 34, 14012−14021
pubs.acs.org/Langmuir

Adhesion of *Marinobacter hydrocarbonoclasticus* to Surfactant-Decorated Dodecane Droplets

Narendra K. Dewangan and Jacinta C. Conrad*

Department of Chemical and Biomolecular Engineering, University of Houston, Houston, Texas 77204-4004, United States

Supporting Information

ABSTRACT: We investigate the effect of interfacial properties on the adhesion of bacteria at oil/water interfaces using confocal microscopy. Surfactant-decorated dodecane droplets of diameter 20−60 μm are generated using a coflow microfluidic device, introduced into an aqueous saline suspension of *Marinobacter hydrocarbonoclasticus* bacteria, and imaged in 3-D over time. Using image analysis algorithms, we determine the number of bacteria adhering at oil/water interfaces over time in the presence of dioctyl sodium succinate (DOSS), a component of the dispersant used in oil-spill recovery. The adsorption of bacteria at the oil/water interface follows Langmuir first-order kinetics for all droplet sizes, with the greatest areal number density of bacteria adhered to the smallest droplets. We vary the surfactant type [DOSS, dicyclohexyl sodium sulfosuccinate, dibutyl sodium sulfosuccinate, cetyltrimethylammonium bromide, and Tween 20] and concentration and examine the effects on long-time adhesion of bacteria. For a fixed droplet size, the areal density of bacteria at the interface decreases with increasing surfactant concentration because of a reduction in oil/water interfacial tension that increases the free energy of adhesion of the bacterium.

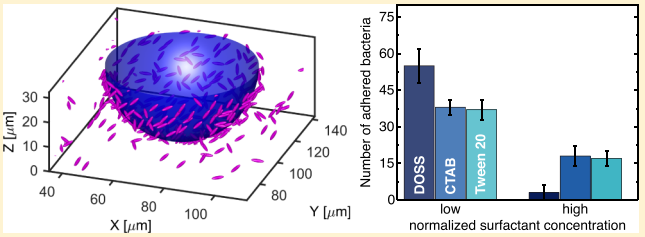

INTRODUCTION

Dispersed hydrocarbons are widely found in marine environments, emerging naturally from oil seeps and as an unintended consequence of petroleum extraction and transportation processes.[1] Thus, many marine bacteria can degrade hydrocarbons.[2−8] Indeed, the surprisingly rapid disappearance in the 2010 Deepwater Horizon spill is thought to be because of bacterial biodegradation.[9−11] The efficacy of biodegradation depends, in part, on the bioavailability of dispersed oil to bacteria. In a typical oil spill scenario, dispersants such as COREXIT EC9500A that contain one or more surfactants[12] are applied near the wellhead and on the water surface[13] to speed up biodegradation.[14−17] Dispersants decrease the interfacial tension (IFT) between the oil and water phases, reducing the Gibbs free energy[18,19] and leading to smaller droplets. Dispersants thus increase the surface area per unit volume and hence the bioavailability of the oil.[7] Because bacterial adhesion to the oil/water interface can promote biodegradation, it is important to understand how surfactants affect adhesion of bacteria at these interfaces.[20−23]

From a thermodynamic perspective, the surface energies of bacteria and the two phases determine the extent of adhesion to oil/water interfaces.[24−26] Briefly, bacteria adhere to the oil/water interface when the sum of the surface energies is lower with the bacterium at the oil/water interfaces than it is with the bacterium entirely in the aqueous phase.[27,28] Surfactants reduce the surface energy of liquid/liquid and bacteria/liquid interfaces, depending on the length and branching of the hydrocarbon chain and on the partitioning of surfactant molecules between the bulk phase and the interface.[29,30] The curvature of the interface between oil droplets and water alters the volume available to surfactant tails and thus modifies the free energy of adsorption in the presence of surfactants,[31] complicating predictions of the adsorption of bacteria to curved oil/water interfaces.

Here, we investigate the effect of interfacial properties on adhesion of hydrocarbon-degrading *Marinobacter hydrocarbonoclasticus* at oil/water interfaces. Using co-flow microfluidic devices, we prepare monodispersed dodecane/water emulsions with drop sizes of 20−60 μm, stabilized with various surfactants. Using confocal microscopy and bacteria-tracking algorithms, we first quantify the number of bacteria adhering at the oil/water interface over time for drops stabilized by dioctyl sodium sulfosuccinate (DOSS), a component of the COREXIT dispersant used in oil spill remediation and used in a variety of emulsification applications. Adhesion of bacteria follows first-order Langmuir kinetics, with a time constant that increases with the drop size. Surprisingly, the areal coverage of bacteria on small 20 μm droplets is larger than that on larger droplets. We subsequently examine the long-time adsorption bacteria on interfaces stabilized by various surfactants, comparing DOSS to two other anionic sodium sulfosuccinates [dibutyl sodium sulfosuccinate (DBSS), dicyclohexyl sodium sulfosuccinate (DCHSS)] as well as to two other surfactants [cationic cetyltrimethylammonium bromide (CTAB), nonionic Tween 20)]. For all surfactants, increasing the surfactant

Received: June 18, 2018
Revised: October 22, 2018
Published: October 24, 2018

DOI: 10.1021/acs.langmuir.8b02071
Langmuir 2018, 34, 14012−14021

concentration at a fixed droplet size reduces the IFT and bacterial adhesion. The type and charge of the surfactant also affect the extent of equilibrium adsorption, with fewer bacteria adhering to anionic (DOSS, DCHSS) interfaces than to CTAB or Tween 20-decorated interfaces at high normalized surfactant concentrations. Our results suggest that the use of surfactants may have competing effects on bacterial adhesion: the increase in adhesion due to a decrease in the droplet size contrasts with the reduction in adhesion because of the lower oil/water IFT.

MATERIALS AND METHODS

Chemicals. Hydrogen peroxide 30% (Macron), sulfuric acid 98% (EMD Millipore), potassium hydroxide (Sigma-Aldrich), methanol (Sigma-Aldrich), acetic acid (EMD Millipore), 3-aminopropyl trimethoxysilane (APTES, Gelest), biotin-mPEG (5000 Da, ThermoFisher), biotin-PEG-SVA-5000 (5000 Da, ThermoFisher), sodium bicarbonate (Sigma-Aldrich), dodecane (>99%, Sigma), DOSS (≥97%, Sigma-Aldrich), DBSS (as received, Sigma-Aldrich), DCHSS (≥98%, Sigma-Aldrich), CTAB (≥99%, Sigma-Aldrich), Tween 20 (ThermoFisher), Zobell marine broth 2216 (HiMedia lab), sodium pyruvate (Amresco), SYTO9 (ThermoFisher), Nile red (Sigma-Aldrich), sodium chloride (Macron), diiodomethane (Sigma-Aldrich), ethylene glycol (Sigma-Aldrich), acetone (BDH), and ethanol (100%, Decon Labs) were used as received. The chemical structures of the five surfactants are shown in Figure 1.

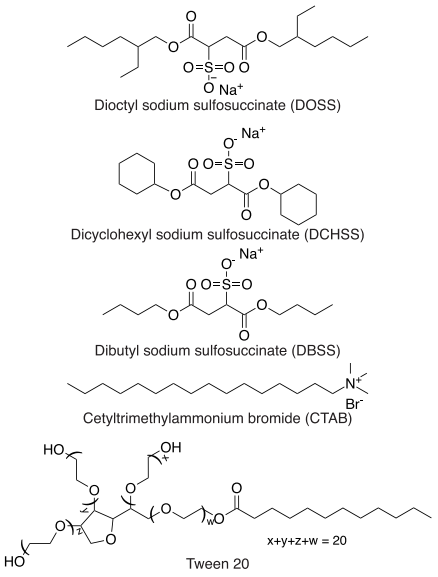

Figure 1. Molecular structure of surfactants used in this study.

Co-flow Microfluidic Device Fabrication. To prepare aqueous emulsions of dodecane with a controlled droplet size, we fabricated co-flow glass capillary microfluidic devices. The device consisted of two coaxially aligned glass capillaries,[32,33] as shown in Figure 2a. The square outer capillary (Vitrocom) had an outer diameter of 1 mm, an inner diameter of 0.90 mm, and a length of 50 mm. The circular inner capillary (Vitrocom) had an outer diameter of 0.87 mm and an inner diameter of 0.70 mm. A dual-stage glass micropipette puller (PC-10, Narishige) was used to generate tapered inner capillaries with a taper length of ∼5 mm and an opening diameter of 5 μm. The outer capillary was also pulled to create a constriction of the inner diameter 120−150 μm and length 10 mm near its midpoint. The inner capillary was inserted within the outer capillary and aligned coaxially near the constriction at the midpoint of the outer capillary. The inlet and outlet were coupled to 18 gauge blunt needles (BD) by using UV adhesive (NOA 68T, Norland), with a glass slide (75 mm × 50 mm,

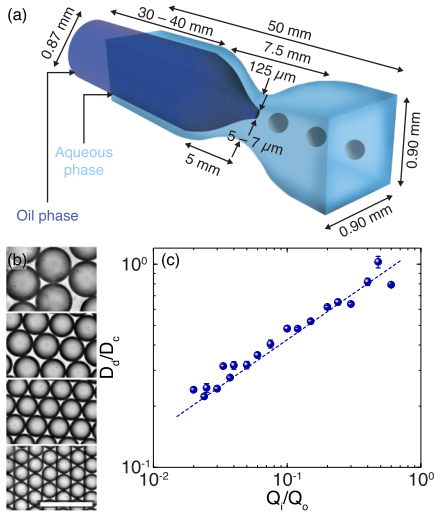

Figure 2. (a) Schematic of the glass-based co-flow microfluidic device used to prepare monodisperse dodecane-in-water emulsions. (b) Brightfield micrographs of monodisperse dodecane-in-water emulsions, stabilized by DOSS at 35 ppm, with drop diameters of 72, 50, 40, and 31 μm, obtained at outer fluid flow rates of 500, 1000, 1500, and 3000 μL min^{-1}, respectively. Scale bar is 100 μm. (c) Normalized droplet size (D_d/D_c) as a function of inner to outer fluid flow rate (Q_i/Q_o). Drop size (D_d) is normalized by the inner diameter of the outer capillary (D_c) measured near the tip location of the inner capillary. Dashed line indicates the fit to eq 1 [ref 34]. Error bars indicate the standard deviation of droplet diameters in a single micrograph, confirming that the emulsions are monodisperse.

Corning) as a supporting base. Tygon tubing (0.03″ ID, Cole-Parmer) was used for all inlet and outlet connections.

Preparation of Oil-In-Water Emulsions. Monodisperse emulsions of dodecane in Milli-Q water (18.2 MΩ·cm) were prepared using the co-flow microfluidic devices.[32] Dodecane droplets were stabilized in water using one of five surfactants: dioctyl sodium sulfosuccinate (DOSS, at concentrations of 2−360 ppm in the aqueous phase), DBSS (1300−130 000 ppm in the aqueous phase), DCHSS (290−29 000 ppm in the aqueous phase), CTAB (2−80 ppm in the aqueous phase), or Tween 20 (1.5−150 ppm in the aqueous phase). The inner oil phase and the outer aqueous phase were dispensed through two gas-tight Luer lock syringes (Hamilton; 2.5 mL inner, 100 mL outer) at constant flow rates by using two syringe pumps: NE-1002X New Era for inner fluid, and Fusion 200 Chemix for the outer fluid. The device was operated at outer flow rates of 50−2000 μL min^{-1} and inner flow rates of 5−25 μL min^{-1}. As-prepared emulsions were stored at 4 °C in dark and used within one week.

Preparation of Glass Capillaries for Imaging. Thin rectangular borosilicate capillaries (0.1 mm height × 1 mm width × 50 mm length, 0.07 mm wall thickness, Vitrocom) were used as sample chambers in imaging experiments. To minimize adhesion of bacteria and prevent wetting of oil droplets, the inner capillary surface was functionalized with polyethylene glycol (PEG) brushes. To prepare the surface for functionalization, capillaries were cleaned with water and acetone, and subsequently treated with 1 M KOH solution and with piranha solution; subsequently, the cleaned capillary was functionalized with APTES and then with PEG (5000 Da).[35] The water contact angle measured on a PEGylated glass slide was 32 ± 2° for three replicates.

Bacteria Strain. *M. hydrocarbonoclasticus* is an extremely halotolerant marine bacterium that is able to degrade both cyclic- and noncyclic alkanes,[36] and increases in abundance in both marine environments[37] and in beach sands[4] after an oil spill. *M. hydrocarbonoclasticus* (ATCC 49840) was obtained from Dr. Douglas Bartlett (Scripps Institute of Oceanography, UCSD). The strain was stored in Zobell marine broth 2216 (Difco)/50% glycerol at −70 °C.

DOI: 10.1021/acs.langmuir.8b02071
Langmuir 2018, 34, 14012−14021

M. hydrocarbonoclasticus, 2−3 μm in length and 0.3−0.6 μm in diameter, is motile in synthetic medium supplemented with NaCl at concentrations of 0.6−1.0 M;[36] we confirmed visually, using optical microscopy, that this strain was not motile in the conditions of this study.

Growth Conditions. *M. hydrocarbonoclasticus* was streaked from a frozen stock on a marine agar plate (37.4 g L^{-1} marine broth, 10 g L^{-1} sodium pyruvate, 15 g L^{-1} agar) and incubated at 30 °C for 48 h. A single colony selected from the plate was inoculated into 20 mL of culture media (37.4 g L^{-1} marine broth and 10 g L^{-1} pyruvate) and incubated for 20 h in an orbital incubator shaker (New Brunswick Scientific) at 200 rpm and 30 °C. Finally, a subculture was prepared by inoculating 75 μL of the principal culture into 20 mL of culture media and grown to a late exponential phase in an orbital incubator shaker at 30 °C and 200 rpm for 20 h.

Zeta Potential and Surface Energy. For surface characterization, *M. hydrocarbonoclasticus* cells were grown to the late exponential phase. Bacteria samples (20 mL) were centrifuged at 5000*g* for 10 min in a Sorvall ST 16 Centrifuge (Thermo Fisher Scientific). The supernatant solution was removed and the pellet was twice resuspended in 20 mL Milli-Q water and centrifuged for cleaning. After cleaning, the pellet was resuspended in Milli-Q water. The final optical density (OD) was adjusted to 0.04 (Laxco DSM-Micro Cell Density Meter, 600 nm) with Milli-Q water.

The zeta potential of the bacteria, measured using a Nicomp 380 ζ-potential analyzer, was −45 ± 3 mV (Table S1). The zeta potential of the bacteria did not markedly change in the presence of surfactants (Table S2). For measurements of the surface energy, the resuspended bacteria sample (OD 1.0) in Milli-Q water was filtered through cellulose acetate membrane filters (pore diameter 0.45 μm, Advantec) under vacuum (100 mm Hg below atmospheric pressure) using a GEM 8890 vacuum pump (Welch).[27,38,39] The filters were attached to glass slides (75 mm × 50 mm) using dental wax (Electron Microscopy Sciences) to ensure that the surface remained flat. The contact angles for three liquids (Milli-Q water, ethylene glycol, and diiodomethane) were measured on the lawns using a DataPhysics OCA 15EC goniometer. The surface energy of the *M. hydrocarbonoclasticus* bacteria, 23 ± 1 mN m^{-1}, was calculated from inbuilt software using the method of Wu.[40,41] Contact angle and surface energy data are provided in Table S3.

Interfacial Tension. To determine the IFT as a function of surfactant concentration, solutions of various surfactants (DOSS, DCHSS, DBSS, CTAB, and Tween 20) were prepared in 5 g L^{-1} NaCl in Milli-Q water. Approximately 3 mL of surfactant solution was taken into a cuvette. Dodecane was dispensed through a U-shaped needle into a surfactant solution-filled cuvette, and a video (25 fps) was captured of the drop shape using a DataPhysics OCA15EC goniometer. At least three replicates were examined for each concentration. The IFT was determined from the radius of curvature of the drop using the Young−Laplace equation.[42,43]

Determination of the Critical Micelle Concentration Using Fluorescence Method. Surfactant solutions at various concentrations were prepared in Milli-Q water with 5 g L^{-1} NaCl. Nile red (excitation/emission maxima ∼552/636 nm, Sigma-Aldrich) was added to each surfactant solution at a concentration of 0.1 mg mL^{-1} and each solution was vigorously vortexed for 5−10 min to solubilize the dye with micelles present in the solution.[44] The solution was vortexed for 1 min every hour. After 3 h, 200 μL of each solution were pipetted into a 96-well plate (Nunc MicroWell 96-Well Optical-Bottom Plates with Polymer Base) and the fluorescence intensities were measured using a SpectraMax Gemini EM Microplate Spectrofluorometer. The intersection of the lines fit to the fluorescence intensity at low and at high surfactant concentration yielded the critical micelle concentration (cmc) value of the surfactant in the presence of 5 g L^{-1} NaCl in water.

Imaging of Cells Near Dodecane−Water Interfaces. For imaging experiments, cells were harvested at the late exponential phase. For fluorescence imaging, 140 μL of the cell suspension were mixed with 860 μL of saline solution (10 g L^{-1} NaCl) or 860 μL of synthetic sea water (SSW; L^{-1}, in distilled water: tris(hydroxymethyl amino methane), 12.1; KCl, 0.75; $CaCl_2$, 1.5; NH_4Cl, 3.47; $MgSO_4 \cdot 7H_2O$, 6.16; $MgCl_2 \cdot 6H_2O$, 5.08; NaCl, 11.7, pH 7.5 with 10 M HCl; note that 2 and 4 mL of aqueous solutions of iron sulphate (0.1% w/v) and sodium phosphate (10%, w/v), respectively, were added to SSW immediately before use), both containing the fluorescent stain SYTO9 (1 μL per 1 mL of cell suspension). These suspensions were incubated at room temperature in the dark for 5−10 min. Dodecane/water emulsion (200 μL) was added into a 1.5 mL Eppendorf tube containing 200 μL of the stained cell suspension. Importantly, to preserve the droplet size the resultant oil/water emulsion was not strongly mixed. 6.5 μL of this suspension, which had a final NaCl concentration of 5 g L^{-1}, was injected into a glass microfluidic channel and both ends of the channel were sealed with vacuum grease. Experiments were run in the limit of very low concentration of emulsion droplets (volume fraction ϕ = 0.003−0.01), so that the bacteria were at excess.

Bacteria were imaged in 3-D over time as they attached to the oil/water interface using a VT-Infinity (Visitech, Sunderland, UK) confocal microscope. The confocal scanhead was mounted on an inverted microscope (Leica Microsystems DM4000) equipped with a 40× oil-immersion lens (HCX PL APO, NA 1.25−0.75). An excitation wavelength of 488 nm was used to excite the SYTO9 stain. To generate a 3-D image stack, we acquired sequential 2-D images over 40, 60, 70, and 80 μm (spacing Δz = 0.31 μm) for oil droplets of diameter 20, 40, 50, or 60 μm, respectively. 3-D stacks were acquired at times t = 5, 15, 30, 60, 90, 120, 150, and 180 min after the cell suspension was added to the emulsion and loaded into the capillary. Each experiment was repeated with at least three independent cultures.

To assess the long-time adhesion of bacteria to oil/water interfaces as a function of the surfactant concentration, emulsions containing dodecane droplets of diameter 20 or 50 μm were added into cell suspensions and loaded into capillaries. The loaded capillaries were incubated at room temperature in the dark for at least 90 min to reach equilibrium (as determined from the time experiments), and z-stack images were acquired for three different droplets in each sample. This experiment was replicated three times at each surfactant concentration for droplets of diameter 20 and 50 μm for DOSS (2, 6, 20, 60, and 180 ppm), DBSS (670 and 67 000 ppm), DCHSS (145 and 14 500 ppm), CTAB (1, 2, 5, 15, and 40 ppm), and Tween 20 (1, 2, 7, 22, and 74 ppm). The centroid and orientation of each cell near the oil/water interface were determined using a MATLAB algorithm based on least-square fitting of backbone of cells in 3D.[45,46] We counted only those cells on the lower hemisphere of the drop to avoid any noisy data associated with cells interacting with the top surface of the microcapillary channel. We confirmed that bacteria in all experiments except CTAB at 1.0 cmc remained viable by streaking postexperiment cells onto agar plates and observing growth (Supporting Information).

■ RESULTS AND DISCUSSION

Monodisperse Emulsion Droplets Using Microfluidics. We generate monodisperse emulsions of dodecane in deionized (DI) water using a co-flow capillary microfluidic device (Figure 2a). The device is operated in the jetting regime, in which a thin jet of liquid is formed at the inner capillary tip and is eventually broken into droplets by the Rayleigh−Plateau instability.[47,48] The jet diameter and the droplet diameter depend on the viscous drag of outer fluid, which can be varied through the flow rate of the outer fluid. We thus tune the diameter of dodecane droplets from 20 to 300 μm in water by varying the outer fluid flow rate from 3000 to 500 μL min^{-1} (Figure 2b). These droplet diameters are typical of those measured in the presence of dispersants in the Deepwater Horizon Spill in 2010.[49]

The droplet diameter D_d, normalized by the diameter of the outer capillary (D_c) at the location of the tip of the inner capillary tip, increases as a power law with the ratio of the inner

DOI: 10.1021/acs.langmuir.8b02071
Langmuir 2018, 34, 14012−14021

and outer fluid flow rates (Q_i/Q_o) with slope ~0.5 (Figure 2c). The normalized drop diameter changes with the normalized flow rate as predicted for the jetting regime[34]

$$\frac{Q_i}{Q_o} = \frac{\eta_o}{\eta_i}\frac{x^4}{(1-x^2)^2} + \frac{2x^2}{(1-x^2)} \quad (1)$$

where $x = D_d/D_c$, Q_i and Q_o are the fluid flow rates of the inner and outer fluids, and η_i and η_o are the viscosities of the inner and outer fluids. This equation was derived in ref 34 by solving the Navier–Stokes equations assuming no-slip boundary conditions, a continuous shear stress at the interface, and an interfacial pressure difference given by the Laplace equation. The power-law behavior arises in our experiments because the first term on the right-hand side of eq 1 is negligible and $1 - x^2 \approx 1$.

Time-Dependent Adsorption of Bacteria at Interfaces. Confocal imaging reveals that the adhesion of *M. hydrocarbonoclasticus* bacteria to DOSS-stabilized dodecane droplets (in solutions of final salt concentration 5 g L^{-1} NaCl) depends on droplet size and time (Figure 3). Using tracking

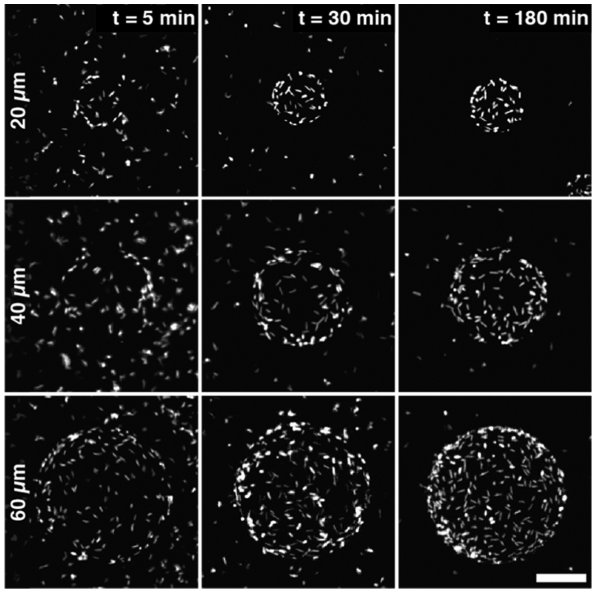

Figure 3. 2-D projections of 3-D confocal micrographs of bacteria adhering at dodecane/water interfaces for droplets of diameter 20, 40, and 60 μm at 5, 30, and 180 min after inoculation of bacteria into the o/w emulsion. Scale bar is 20 μm. In all experiments DOSS (18 ppm final concentration) is added to the aqueous phase to stabilize the dodecane droplets in saline solution (final salt concentration 5 g L^{-1} NaCl).

algorithms, we quantify the number of bacteria on the interface of dodecane droplets of diameter 20, 40, and 60 μm. For all droplet sizes, the number of *M. hydrocarbonoclasticus* bacteria adhered at a dodecane/water interface initially increases with time and then saturates on longer time scales (Figure 4a). No significant change in the number of adhered cells is observed after 3 h. As a control experiment, we observe nearly no adhesion of negatively-charged surfactant-stabilized polystyrene (diameters 0.79 and 2 μm; zeta potentials -46 ± 2 and -41 ± 2 mV) or poly(methylmethacrylate) (diameter 1.2 μm; zeta potential -38 ± 1 mV) particles at similar number concentrations and over similar time scales (Table S5). Because *M. hydrocarbonoclasticus* bacteria are not motile

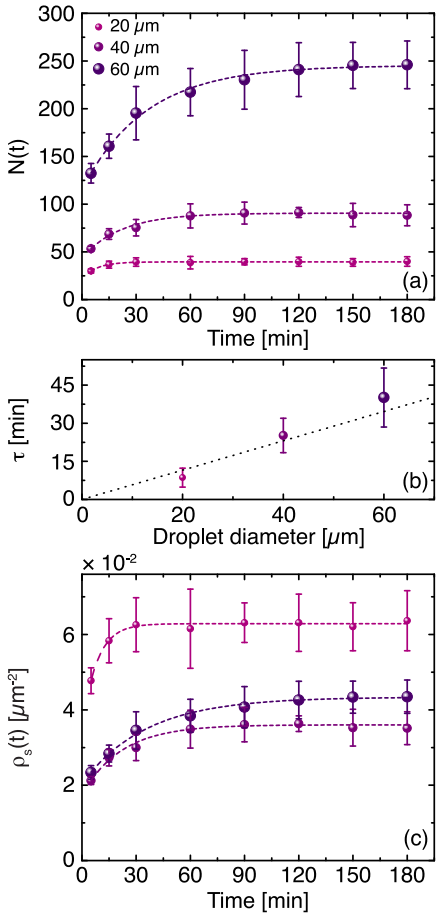

Figure 4. Number of bacteria at the dodecane/water interface $N(t)$ as a function of time for droplets of diameter 20, 40, and 60 μm. (b) Time constant of the first-order Langmuir kinetics model, extracted from a fit to eq 2, for 20, 40, and 60 μm dodecane droplets. (c) Number of cells per unit surface area $\rho_s(t)$ as a function of time for 20, 40, and 60 μm dodecane droplets. In all experiments DOSS (18 ppm final concentration) is added to the aqueous phase to stabilize the dodecane droplets in saline solution (final salt concentration 5 g L^{-1} NaCl). Error bars represent standard deviation from three independent cultures. Dashed lines in (a,c) represent fits to the first-order Langmuir kinetics model (eq 2); the dotted line in (b) represents a linear fit through the origin.

under these experimental conditions, the transport of cells to the interface is driven by diffusion; on long time scales cells become depleted near the oil/water interface, leading to a plateau in adsorption.

This scenario suggests that the number of bacteria on the dodecane/water interface at time t, $N(t)$, can be modeled using the Langmuir first-order kinetics model[50−52]

$$N(t) = N_\infty - (N_\infty - N_0)e^{-t/\tau} \quad (2)$$

where N_0 and N_∞ are the number of cells that initially (at the earliest time point, as soon as possible after bacteria are inoculated into the oil/water emulsion) and finally (as $t \to \infty$) adhere, respectively, and τ is the characteristic time for the interface to saturate. The time constants τ extracted from fits to eq 2 increase linearly with the droplet diameter, indicating that bacteria adhere more rapidly to smaller droplets (Figure 4b). This linear dependence on droplet diameter is consistent with a kinetic model for the time required, in irreversible Langmuir adsorption, to reach a fractional coverage within a

DOI: 10.1021/acs.langmuir.8b02071
Langmuir 2018, 34, 14012−14021

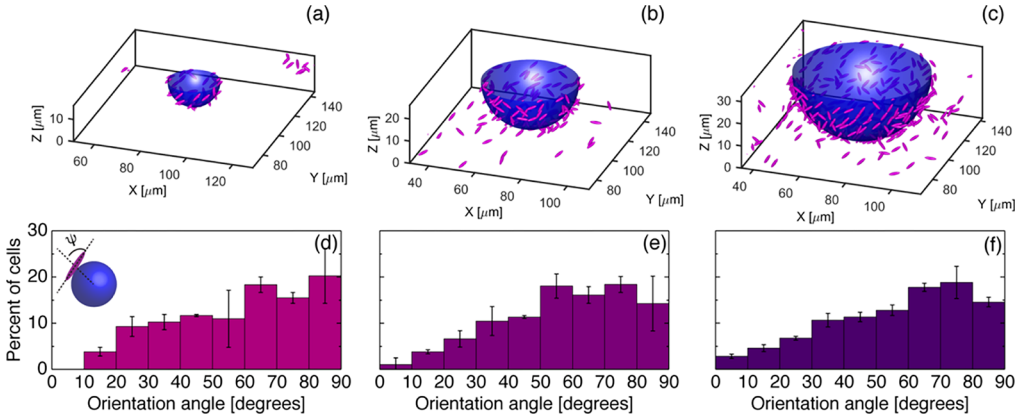

Figure 5. (a–c) Representative 3-D renderings of the location and orientation of bacteria around dodecane droplets in saline solution (final salt concentration 5 g L^{-1} NaCl) of diameter (a) 20, (b) 40, and (c) 60 μm. (d–f) Distribution of the orientation angle ψ at which bacteria adhere to the interface for dodecane droplets of diameter (d) 20, (e) 40, and (f) 60 μm. ψ is defined by the angle between the cell backbone and the normal on the droplet that passes through the cell centroid, as indicated in the inset to Figure 5d.

factor h of the equilibrium value on a sphere,[53] $t_h = -\frac{RK\gamma_s \ln h}{D(1+KC_0)^2}$, where K is an affinity constant, R is the radius of the droplet, D is diffusivity of cells, C_0 is cell concentration, and γ_s is the number of adsorption sites per unit surface area. The applicability of this model requires that bacteria are in excess, that the droplet is homogenous, and that K and γ_s are constant across the different drop sizes, which are reasonable assumptions for our experiments.

The good fit of the data to eq 2 confirms that the dynamics of adhesion for nonmotile bacteria obey first-order Langmuir kinetics. The value of N_∞ increases with the droplet radius, as expected because the droplet surface area also increases. We therefore normalize by the droplet hemisphere surface area to obtain the interfacial areal density of bacteria $\rho_s(t) = N(t)/2\pi R^2$. The areal density is greatest for the smallest 20 μm droplets but is constant (within measurement error) for the two larger droplets (Figure 4c). This result suggests that decreasing the oil drop size may provide at least two mechanisms to increase accessibility to bacteria: by increasing the surface area per volume available for adhesion (Figure S1), and by enhancing cell adhesion on smaller droplets.

We next examine the orientation of bacteria on the oil/water interface, defined as the angle between the bacterial body and the local surface normal. For all droplet sizes, the majority of adherent cells are oriented at an angle >60° to the surface normal (Figure 5) and align roughly parallel to the interface. The parallel orientation of the cells provides one route to minimize the energy cost due to IFT.[54,55] A significant fraction of cells, however, orient at lower angles with respect to the surface normal. Although bacteria with relatively hydrophobic surface regions can uniformly orient perpendicular to fluid/fluid interfaces,[56] the distribution of orientations suggests contributions from additional factors.

The thermodynamic model of adhesion indicates that the energy cost to place a smooth, homogeneous bacterium at an oil/water interface is given by

$$\Delta E = -\sigma_{ow}(A_{ow} - A_{bo}\cos\theta_c) \quad (3)$$

where σ_{ow}, σ_{bw}, and σ_{bo} are respectively the oil/water, bacteria/water, and bacteria/oil IFTs, A_{bo} is the portion of the bacterium immersed in the oil phase, A_{ow} is the portion of the interface removed by the adsorbed bacterium, and θ_c is the water contact angle in oil of the adsorbed bacterium (Figure 6).[57,58] Here, we assume that the only change that occurs upon

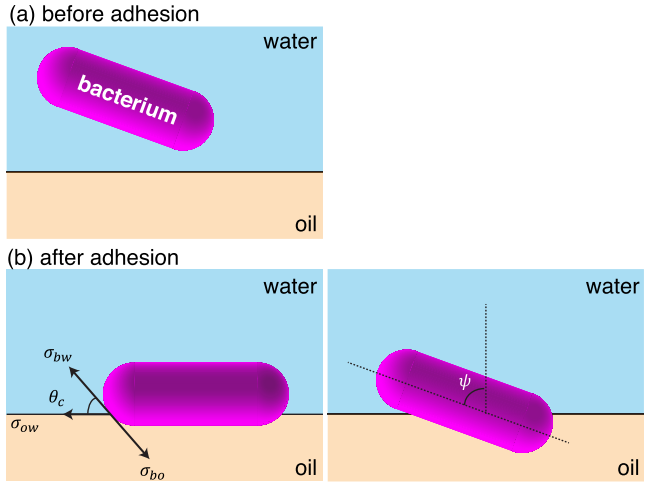

Figure 6. Schematic illustration of bacteria adsorbed (a) before adhesion in water and (b) after adhesion for planar or tilted orientations at an oil/water interface.

addition of surfactants is a decrease in the oil/water IFT (σ_{ow}) (a derivation of eq 3 is provided in the Supporting Information). Chemically isotropic but geometrically anisotropic colloidal particles, such as ellipsoids[59,60] or cylinders,[61] typically align along an interface and thereby maximize the oil/water interfacial area displaced by the particles. The fact that many bacteria do not orient parallel to the interface suggests that the assumptions underlying the thermodynamic model do not all hold. Indeed, particles with chemical and/or topographic[62,63] surface heterogeneity can exhibit a broad distribution of contact angles[64] and adsorb in metastable configurations.[65−68] Although our results suggest that bacteria preferentially adsorb in the thermodynamically-favored configuration, the broad distribution of orientations likely reflects their surface heterogeneity.

Equilibrium Adhesion Isotherms. The adhesion dynamics reported in Figure 4 follow first-order Langmuir kinetics, with the extent of adhesion differing between the smallest and the larger drops. We next examine the equilibrium adhesion of

DOI: 10.1021/acs.langmuir.8b02071
Langmuir 2018, 34, 14012−14021

M. hydrocarbonoclasticus bacteria on curved dodecane/water interfaces. For a series of three commercially available anionic sodium sulfosuccinates [DBSS (C-4), DCHSS (cyclo C-6) , and DOSS (C-8)], we quantify the number of cells adhered on long time scales to surfactant-decorated dodecane/water interfaces at low (C/cmc ≈ 0.01) and high (C/cmc ≈ 1) surfactant concentrations, where cmc indicates the critical micelle concentration determined through fluorimetry (Figure S2). The areal density of bacteria on the dodecane/water interface of a 20 μm droplet stabilized by each of the three sulfosuccinates is the same within experimental error (Figure 7a).[a]

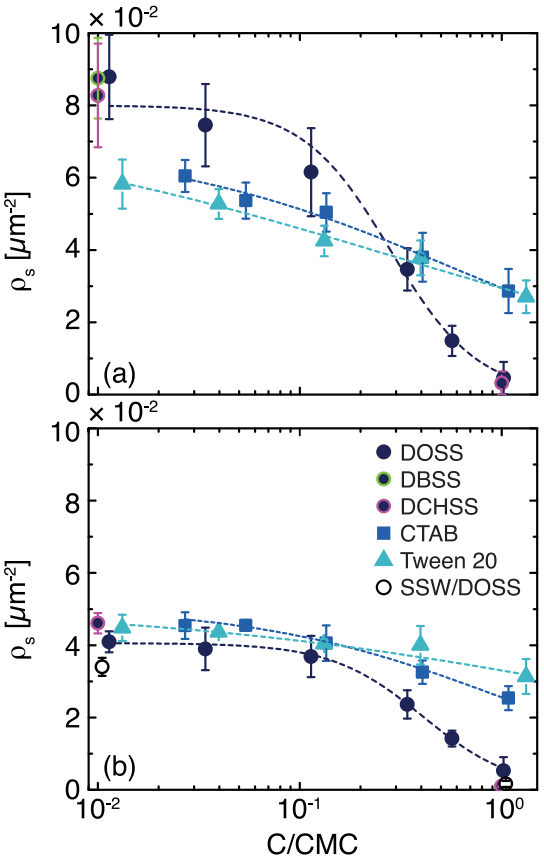

Figure 7. Areal density ρ_s of cells adhering at the dodecane/water (closed) or dodecane/synthetic sea water (open) interface as a function of normalized surfactant concentration C/cmc for drops of diameter (a) 20 or (b) 50 μm. Error bars represent the standard deviation calculated from three independent bacterial cultures.

Next, we quantify the packing efficiency via the surface excess Γ, defined as the number of moles of surfactant molecules per unit interfacial area, and the surface area occupied by a surfactant molecule.[69−73] The surface excess is calculated at the cmc from the dependence of the IFT on the surfactant concentration (Figure 8) via

$$\Gamma = -\frac{1}{nRT}\left(\frac{\partial\sigma}{\partial \ln C}\right)_{T,P} \quad (4)$$

where σ is the IFT of dodecane/water, C is the surfactant concentration, R is the gas constant, T is the temperature, and n = 1 when electrolyte is present. We assume that the surfactant activity coefficient is equal to one. The surface

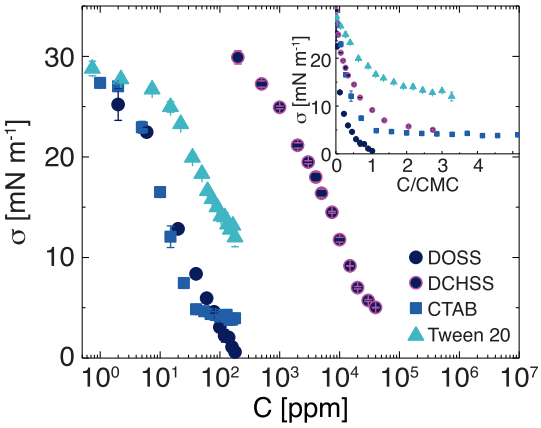

Figure 8. IFT σ between dodecane and water containing 5 g L^{-1} sodium chloride in the presence of various surfactants.

coverage per surfactant molecule is then given by $A_a = \frac{1}{N_A\Gamma}$. The IFT σ initially decreases sharply with an increase in the surfactant concentration, as more surfactant molecules adsorb at the dodecane/water interface; above the cmc, the IFT decreases slowly as the surfactant concentration is further increased (Figure 8). For a similar normalized surfactant concentration, σ for DCHSS is much higher than that of DOSS. Furthermore, σ for DOSS falls to near-zero at its cmc but remains finite up to (at least) c/cmc = 3 for DCHSS. The surface area per DOSS molecule, 78 ± 2 Å^2, is in good agreement with literature values[74] and is larger than that for DCHSS, 54 ± 2 Å^2 (Table 1). Because the areal density of

Table 1. Surface Coverage per Molecule at cmc of Different Surfactants

surfactant	surface excess [10^{-6} mol m^{-2}]	surface area per molecule [Å^2]
DOSS	2.12 ± 0.05	78 ± 2
Tween 20	2.34 ± 0.09	71 ± 3
CTAB	2.74 ± 0.24	61 ± 5
DCHSS	3.26 ± 0.07	54 ± 2

bacteria is identical for the three sodium sulfosuccinates, despite distinct values of the IFT and the surface area per molecule, we conclude that the electrostatic repulsion of the negatively-charged bacteria from the negatively-charged surfactants affects bacterial adhesion to these surfactant-decorated dodecane/water interfaces. Moreover, this effect is likely partly kinetic (i.e. through the double-layer force) because adhesion cannot be predicted solely from the IFT (i.e. thermodynamics).

We next compare results on bacterial adhesion from DOSS to those obtained for two other common surfactants used in bacterial studies,[75] nonionic Tween 20 and cationic CTAB. The areal density of bacteria on the oil/water interface decreases for each surfactant as its concentration is increased (Figure 7). This trend holds both for larger 50 μm droplets, for which the final number of adhered bacteria scales with the interfacial surface area, and for small 20 μm droplets, which exhibit anomalously high adhesion. The areal densities (and hence number) of bacteria adhered to drops stabilized by CTAB and by Tween 20 are similar for a given droplet diameter, and are larger than the number of bacteria adhered to DOSS-decorated dodecane/water interfaces near cmc.

DOI: 10.1021/acs.langmuir.8b02071
Langmuir 2018, 34, 14012−14021

We again compare the IFT of surfactant-decorated dodecane/water interfaces and the surface area per molecule as a function of surfactant concentration. The high-concentration values of σ are markedly different for CTAB and Tween 20 compared to DOSS: σ for CTAB and Tween 20 remains nonzero even at surfactant concentrations of up to 180 ppm, whereas σ for DOSS decreases to near zero at its cmc value. Indeed, the areal density of bacteria adhering at droplet interfaces decreases concomitant with σ for all surfactants (Figure 9). These results are consistent with earlier studies

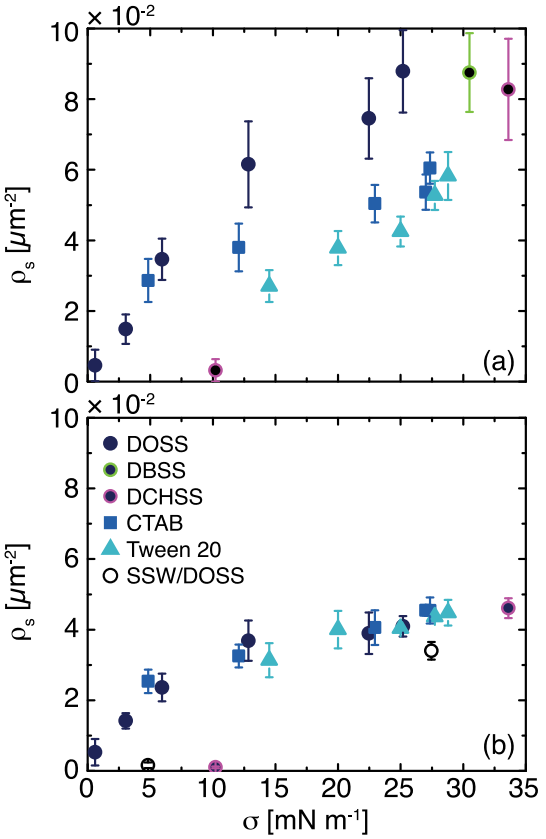

Figure 9. Areal density ρ_s of bacteria at the dodecane/water (closed) or dodecane/synthetic sea water (open) interface as a function of the IFT σ for droplet diameters of (a) 20 or (b) 50 μm. Error bars represent the standard deviation from three independent bacteria cultures.

reporting a decrease in adhesion of bacteria on solid surfaces as the surface tension is decreased,[24,76,77] such that the free energy of adhesion becomes less negative.[27,78] For 50 μm droplets, the areal density of adhered bacteria nearly collapses onto a universal curve with σ for DOSS, CTAB, and Tween 20; for 20 μm droplets, however, the number of bacteria does not cleanly collapse with σ. This result, like that in Figure 4, is consistent with droplet-size-dependent adhesion of bacteria.

Finally, we compare the surface excess and surface area per molecule for the different surfactants. DOSS has the highest surface area per molecule of the four surfactants examined; the surface area per molecule increases in the order DCHSS < CTAB < Tween 20 < DOSS. The high surface area per molecule of DOSS is because of its two branched linear chains, which increases its emulsification efficiency.[74,79] The efficiency of coverage is further enhanced due to counterions in solution that occupy the space between the head groups.[79] At the cmc; however, bacterial adhesion onto a 20 μm droplet increases in the order DCHSS ≈ DOSS < CTAB ≈ Tween 20, indicating that the surface area of the surfactant molecule does not strongly affect bacterial adhesion.

Together, the results presented in Figures 7−9 suggest that both IFT and electrostatic interactions affect the adhesion of *M. hydrocarbonoclasticus* to dodecane/water interfaces in saline solution. The areal density of bacteria on 50 μm droplets increases with IFT across the range of surfactants tested (Figure 9b). Pronounced differences between the areal densities on smaller 20 μm droplets stabilized by various surfactants; however, indicate that nonthermodynamic factors also contribute to adhesion. To understand the origin of these differences, we measured the zeta potential of surfactant-stabilized emulsions (DOSS, CTAB, Tween 20) containing droplets of 20 or 50 μm (Table 2). The magnitude of the zeta potential was greater for the smaller 20 μm droplets than for the 50 μm droplets, consistent with (albeit not proof positive) of an enhanced role for electrostatic interactions in the adhesion of bacteria to these droplets. Likewise, comparison of adhesion on DCHSS- and CTAB-decorated 20 μm droplets suggests contributions from electrostatics. The IFT of droplets stabilized by 1 cmc DCHSS [14 500 ppm] and 1 cmc CTAB [35 ppm] are similar, as are the surface areas per molecule (Table 1), but significantly fewer (negatively-charged) bacteria adhere to the anionic, DCHSS-stabilized dodecane/water interface than to the cationic CTAB-stabilized dodecane/water interface.

Adhesion in Synthetic Sea Water. The ionic strength of the saline solution (86 mM) used in most of our experiments of the experiments is lower than that of sea water (590 mM). We thus also quantify adhesion of *M. hydrocarbonoclasticus* suspended in synthetic sea water to DOSS-decorated dodecane droplets (open symbols in Figures 7 and 9). The adhesion of bacteria to dodecane/synthetic sea water interfaces follows similar trends as those observed for adhesion to interfaces in saline solution: adhesion decreased with increasing DOSS concentration, approaching near-zero at the cmc. The slightly lower adhesion in synthetic seawater at a given DOSS concentration (Figure 7) is likely because of the additional salts; the very low adhesion at the highest DOSS concentration

Table 2. Zeta Potential of Uniform Emulsion Droplets of 20 and 50 μm in Milli-Q Water for Various Surfactants at Three Concentrations[a]

	DOSS		CTAB		Tween 20	
concentration [cmc]	20 μm	50 μm	20 μm	50 μm	20 μm	50 μm
0.01	−79 ± 2	−59 ± 5	70 ± 2	35 ± 4	−12 ± 1	−7 ± 1
0.1	−77 ± 3	−68 ± 3	77 ± 2	54 ± 7	−21 ± 1	−21 ± 1
1.0	−118 ± 2	−100 ± 4	95 ± 3	76 ± 3	−33 ± 1	−55 ± 1

[a]Errors are the standard deviation of 10 runs obtained from measurements on a single sample.

DOI: 10.1021/acs.langmuir.8b02071
Langmuir 2018, 34, 14012−14021

(Figure 9) again reflects the effects of electrostatic repulsions on adhesion.

CONCLUSIONS

We examined the effect of droplet size and surfactant type and concentration on bacterial adhesion at dodecane/water interfaces. Bacteria adhere in slightly greatly areal densities on small droplets of diameter 20 μm, and reach equilibrium coverage more slowly as the droplet size is increased. Bacteria preferentially align parallel to the local oil/water interface, in agreement with expectations from thermodynamics to maximize the displaced interfacial area, but the distribution of angular orientations suggest that bacteria can become kinetically trapped in nonequilibrium orientations. At equilibrium, bacteria adhere more to droplets stabilized by lower concentrations of surfactants. This result is consistent with an increase in the free energy of adhesion because of the decrease in the oil/water IFT (neglecting any changes in bacteria/oil or bacteria/water IFTs). Comparison of adhesion to droplets of various sizes decorated by different surfactants suggests that electrostatics also play a role in determining the number of adhered bacteria, especially for smaller 20 μm droplets.

Overall, these results indicate that surfactants may have contrasting effects on bacterial adhesion to dodecane/water interfaces: for a constant volume of emulsified oil, increasing the surfactant concentration increases the surface area available for bacteria to adhere, but lowers bacterial adhesion energy because of the decrease in IFT. Furthermore, the surface density of adhered bacteria and its dependence on the IFT are different for the smallest 20 μm droplets, consistent with an additional role for electrostatics. These effects should be considered for optimal (i.e. minimal) application of surfactants or dispersants early in an oil spill scenario. On longer time scales, however, oil-metabolizing bacteria may be able to grow on the oil/water interface[80] and further modify the IFT, further complicating predictions of the extent of biodegradation by oil-metabolizing bacteria. In addition, some strains of *M. hydrocarbonoclasticus* are able to produce biosurfactants that aid attachment to the oil/water interface.[81] Finally, the adhesion of nonmotile bacteria to a dodecane/water interface under quiescent conditions studied here represents a simplification of conditions encountered during marine biodegradation: crude oil contains a mixture of aromatic and nonaromatic hydrocarbons; other hydrocarbon-degrading species involved in biodegradation are motile; and even gentle flow alters the behavior of microorganisms.[82] Both flow and motility are likely to modify the interactions of bacteria as they become confined near oil/water interfaces.[83] Very recent experiments suggest that bacterial attachment may be quite different in clean environmental conditions (featuring dissolved organic carbon) and in an oil spill scenario (featuring only hydrocarbons as the carbon source).[84] Future studies examining the effects of growth, bacterial exudates, motility, flow, and organic matter on interfacial adhesion are expected to provide additional insight into the processes influencing biodegradation.

The results reported here have broader implications for technological processes in which bacteria interact with oil/water interfaces. Microfluidically-produced droplets of water in oil, as one example, are increasingly used as controlled microscale reactors for pathogen detection, antibiotic susceptibility, and biotechnological selection, among other emerging applications.[85] Likewise, interactions with hydrocarbon/water interfaces are important for treatment of wastewater.[86] The methods applied here to hydrocarbon-degrading bacteria can be used to optimize and tune the interactions of other bacteria strains with interfaces in these technologically relevant settings.

ASSOCIATED CONTENT

Supporting Information

The Supporting Information is available free of charge on the ACS Publications website at DOI: 10.1021/acs.langmuir.8b02071.

Five tables, three figures, and supporting methods: zeta potential of *M. hydrocarbonoclasticus*; zeta potential of bacteria as a function of surfactant concentration; static water contact angle and surface energy of *M. hydrocarbonoclasticus*; number of bacteria at the dodecane/water interface normalized by volume as a function of time; determination of the cmc for DCHSS, DOSS, CTAB, and Tween 20 in saline solution; determination of the cmc for DOSS in synthetic sea water; pH of surfactant solutions; zeta potential of colloidal particles in DI water; and supporting methods: MATH assay, viability assay, thermodynamic analysis, cmc determination, pH measurements, and colloidal particle adsorption experiments (PDF)

AUTHOR INFORMATION

Corresponding Author

*E-mail: jcconrad@uh.edu.

ORCID

Jacinta C. Conrad: 0000-0001-6084-4772

Notes

The authors declare no competing financial interest.

ACKNOWLEDGMENTS

This research was made possible in part by a grant from The Gulf of Mexico Research Initiative, and in part by the Welch Foundation (E-1869). Data generated for this paper is available on the Gulf of Mexico Research Initiative Information and Data Cooperative (GRIIDC) at https://data.gulfresearchinitiative.org (DOI: 10.7266/N7CR5RZZ). We thank Patrick Cirino for access to his bacteria culture facilities, Douglas Bartlett for bacterial strains and helpful feedback, and five anonymous reviewers for insightful comments and suggestions.

ADDITIONAL NOTE

[a]Because bacteria aggregate at an oil/water interface in the presence of DBSS at its cmc, it is not possible to enumerate bacteria for this condition.

REFERENCES

(1) National Research Council (US) Committee on Oil in the Sea: Inputs, Fates, and Effects. *Input of Oil to the Sea*; National Academies Press: Washington, DC, US, 2003.

(2) Rahman, K. S. M.; Thahira-Rahman, J.; Lakshmanaperumalsamy, P.; Banat, I. M. Towards Efficient Crude Oil Degradation by a Mixed Bacterial Consortium. *Bioresour. Technol.* **2002**, *85*, 257−261.

(3) Brooijmans, R. J. W.; Pastink, M. I.; Siezen, R. J. Hydrocarbon-degrading bacteria: the oil-spill clean-up crew. *Microb. Biotechnol.* **2009**, *2*, 587−594.

DOI: 10.1021/acs.langmuir.8b02071
Langmuir 2018, 34, 14012−14021

(4) Kostka, J. E.; Prakash, O.; Overholt, W. A.; Green, S. J.; Freyer, G.; Canion, A.; Delgardio, J.; Norton, N.; Hazen, T. C.; Huettel, M. Hydrocarbon-Degrading Bacteria and the Bacterial Community Response in Gulf of Mexico Beach Sands Impacted by the Deepwater Horizon Oil Spill. *Appl. Environ. Microbiol.* **2011**, *77*, 7962−7974.
(5) Prince, R. C.; McFarlin, K. M.; Butler, J. D.; Febbo, E. J.; Wang, F. C. Y.; Nedwed, T. J. The Primary Biodegradation of Dispersed Crude Oil in the Sea. *Chemosphere* **2013**, *90*, 521−526.
(6) McFarlin, K. M.; Prince, R. C.; Perkins, R.; Leigh, M. B. Biodegradation of Dispersed Oil in Arctic Seawater at −1 °C. *PLoS ONE* **2014**, *9*, No. e84297.
(7) Prince, R. C. Oil Spill Dispersants: Boon or Bane? *Environ. Sci. Technol.* **2015**, *49*, 6376−6384.
(8) Prince, R. C.; Nash, G. W.; Hill, S. J. The Biodegradation of Crude Oil in the Deep Ocean. *Mar. Pollut. Bull.* **2016**, *111*, 354−357.
(9) Mahmoudi, N.; Porter, T. M.; Zimmerman, A. R.; Fulthorpe, R. R.; Kasozi, G. N.; Silliman, B. R.; Slater, G. F. Rapid Degradation of Deepwater Horizon Spilled Oil by Indigenous Microbial Communities in Louisiana Saltmarsh Sediments. *Environ. Sci. Technol.* **2013**, *47*, 13303−13312.
(10) Bagby, S. C.; Reddy, C. M.; Aeppli, C.; Fisher, G. B.; Valentine, D. L. Persistence and biodegradation of oil at the ocean floor followingDeepwater Horizon. *Proc. Natl. Acad. Sci. U.S.A.* **2016**, *114*, E9−E18.
(11) Bostic, J. T.; Aeppli, C.; Swarthout, R. F.; Reddy, C. M.; Ziolkowski, L. A. Ongoing Biodegradation of Deepwater Horizon Oil in Beach Sands: Insights from Tracing Petroleum Carbon into Microbial Biomass. *Mar. Pollut. Bull.* **2018**, *126*, 130−136.
(12) Place, B.; Anderson, B.; Mekebri, A.; Furlong, E. T.; Gray, J. L.; Tjeerdema, R.; Field, J. A Role for Analytical Chemistry in Advancing our Understanding of the Occurrence, Fate, and Effects of Corexit Oil Dispersants. *Environ. Sci. Technol.* **2010**, *44*, 6016−6018.
(13) Brakstad, O. G.; Nordtug, T.; Throne-Holst, M. Biodegradation of Dispersed Macondo Oil in Seawater at Low Temperature and Different Oil Droplet Sizes. *Mar. Pollut. Bull.* **2015**, *93*, 144−152.
(14) Hamdan, L. J.; Fulmer, P. A. Effects of COREXIT EC9500A on bacteria from a beach oiled by the Deepwater Horizon spill. *Aquat. Microb. Ecol.* **2011**, *63*, 101−109.
(15) Zahed, M. A.; Aziz, H. A.; Isa, M. H.; Mohajeri, L.; Mohajeri, S.; Kutty, S. R. M. Kinetic Modeling and Half Life Study on Bioremediation of Crude Oil Dispersed by Corexit 9500. *J. Hazard. Mater.* **2011**, *185*, 1027−1031.
(16) Chakraborty, R.; Borglin, S. E.; Dubinsky, E. A.; Andersen, G. L.; Hazen, T. C. Microbial Response to the MC-252 Oil and Corexit 9500 in the Gulf of Mexico. *Front. Microbiol.* **2012**, *3*, 357.
(17) Kleindienst, S.; Seidel, M.; Ziervogel, K.; Grim, S.; Loftis, K.; Harrison, S.; Malkin, S. Y.; Perkins, M. J.; Field, J.; Sogin, M. L.; Dittmar, T.; Passow, U.; Medeiros, P. M.; Joye, S. B. Chemical Dispersants can Suppress the Activity of Natural Oil-Degrading Microorganisms. *Proc. Natl. Acad. Sci. U.S.A.* **2015**, *112*, 14900−14905.
(18) Amir, K.; Hossein, A.; Montazer-Rahmati, M. M. The Effect of Sodium Dodecyl Sulfate on Mean Drop Size in a Horizontal Mixer−Settler Extractor. *Canad. J. Chem. Eng.* **2010**, *88*, 101−108.
(19) Xue, Y.-Q.; Yang, X.-C.; Cui, Z.-X.; Lai, W.-P. The Effect of Microdroplet Size on the Surface Tension and Tolman Length. *J. Phys. Chem. B* **2011**, *115*, 109−112.
(20) O'Toole, G.; Kaplan, H. B.; Kolter, R. Biofilm Formation as Microbial Development. *Annu. Rev. Microbiol.* **2000**, *54*, 49−79.
(21) Katsikogianni, M.; Missirlis, Y. F. Concise review of mechanisms of bacterial adhesion to biomaterials and of techniques used in estimating bacteria-material interactions. *Eur. Cell. Mater.* **2004**, *8*, 37−57.
(22) Kim, J.; Park, H.-D.; Chung, S. Microfluidic Approaches to Bacterial Biofilm Formation. *Molecules* **2012**, *17*, 9818−9834.
(23) Persat, A.; Nadell, C. D.; Kim, M. K.; Ingremeau, F.; Siryaporn, A.; Drescher, K.; Wingreen, N. S.; Bassler, B. L.; Gitai, Z.; Stone, H. A. The Mechanical World of Bacteria. *Cell* **2015**, *161*, 988−997.
(24) Absolom, D. R.; Lamberti, F. V.; Policova, Z.; Zingg, W.; van Oss, C. J.; Neumann, A. W. Surface Thermodynamics of Bacterial Adhesion. *Appl. Environ. Microbiol.* **1983**, *46*, 90−97.
(25) Sharma, S.; Conrad, J. C. Attachment from Flow of Escherichia coli Bacteria onto Silanized Glass Substrates. *Langmuir* **2014**, *30*, 11147−11155.
(26) Sharma, S.; Jaimes-Lizcano, Y. A.; McLay, R. B.; Cirino, P. C.; Conrad, J. C. Subnanometric Roughness Affects the Deposition and Mobile Adhesion of Escherichia coli on Silanized Glass Surfaces. *Langmuir* **2016**, *32*, 5422−5433.
(27) Liu, Y.; Zhao, Q. Influence of Surface Energy of Modified Surfaces on Bacterial Adhesion. *Biophys. Chem.* **2005**, *117*, 39−45.
(28) Maestro, A.; Santini, E.; Zabiegaj, D.; Llamas, S.; Ravera, F.; Liggieri, L.; Ortega, F.; Rubio, R.; Guzman, E. Particle and Particle-Surfactant Mixtures at Fluid Interfaces: Assembly, Morphology, and Rheological Description. *Adv. Condens. Matter Phys.* **2015**, *2015*, 917516.
(29) Rekvig, L.; Kranenburg, M.; Hafskjold, B.; Smit, B. Effect of Surfactant Structure on Interfacial Properties. *Europhys. Lett.* **2003**, *63*, 902−907.
(30) Adkins, S. S.; Chen, X.; Nguyen, Q. P.; Sanders, A. W.; Johnston, K. P. Effect of branching on the interfacial properties of nonionic hydrocarbon surfactants at the air-water and carbon dioxide-water interfaces. *J. Colloid Interface Sci.* **2010**, *346*, 455−463.
(31) Farrow, M. R.; Camp, P. J.; Dowding, P. J.; Lewtas, K. The Effects of Surface Curvature on the Adsorption of Surfactants at the Solid-Liquid Interface. *Phys. Chem. Chem. Phys.* **2013**, *15*, 11653−11660.
(32) Utada, A. S.; Fernandez-Nieves, A.; Stone, H. A.; Weitz, D. A. Dripping to Jetting Transitions in Coflowing Liquid Streams. *Phys. Rev. Lett.* **2007**, *99*, 094502.
(33) Shah, R. K.; Shum, H. C.; Rowat, A. C.; Lee, D.; Agresti, J. J.; Utada, A. S.; Chu, L.-Y.; Kim, J.-W.; Fernandez-Nieves, A.; Martinez, C. J.; Weitz, D. A. Designer Emulsions Using Microfluidics. *Materials Today* **2008**, *11*, 18−27.
(34) van Hoeve, W.; Dollet, B.; Gordillo, J. M.; Versluis, M.; van Wijngaarden, L.; Lohse, D. Bubble Size Prediction in Co-Flowing Streams. *Europhys. Lett.* **2011**, *94*, 64001.
(35) Chandradoss, S. D.; Haagsma, A. C.; Lee, Y. K.; Hwang, J.-H.; Nam, J.-M.; Joo, C. Surface Passivation for Single-Molecule Protein Studies. *J. Vis. Exp.* **2014**, *86*, 50549.
(36) Gauthier, M. J.; Lafay, B.; Christen, R.; Fernandez, L.; Acquaviva, M.; Bonin, P.; Bertrand, J.-C. *Marinobacter hydrocarbonoclasticus* gen. nov., sp. nov., a New, Extremely Halotolerant, Hydrocarbon-Degrading Marine Bacterium. *Int J Syst Bacteriol* **1992**, *42*, 568−576.
(37) Gerdes, B.; Brinkmeyer, R.; Dieckmann, G.; Helmke, E. Influence of crude oil on changes of bacterial communities in Arctic sea-ice. *FEMS Microbiol. Ecol.* **2005**, *53*, 129−139.
(38) Reid, G.; Cuperus, P. L.; Bruce, A. W.; van der Mei, H. C.; Tomeczek, L.; Khoury, A. H.; Busscher, H. J. Comparison of Contact Angles and Adhesion to Hexadecane of Urogenital, Dairy, and Poultry Lactobacilli: Effect of Serial Culture Passages. *Appl. Environ. Microbiol.* **1992**, *58*, 1549−1553.
(39) McLay, R. B.; Nguyen, H. N.; Jaimes-Lizcano, Y. A.; Dewangan, N. K.; Alexandrova, S.; Rodrigues, D. F.; Cirino, P. C.; Conrad, J. C. Level of Fimbriation Alters the Adhesion of Escherichia coli Bacteria to Interfaces. *Langmuir* **2018**, *34*, 1133−1142.
(40) Wu, S. Calculation of Interfacial Tension in Polymer Systems. *J. Polym. Sci. C Polym. Symp.* **1971**, *34*, 19−30.
(41) Wu, S. Polar and Nonpolar Interactions in Adhesion. *J. Adhes.* **1973**, *5*, 39−55.
(42) Wu, S. Surface and Interfacial Tensions of Polymer Melts. II. Poly(methyl methacrylate), Poly(n-butyl methacrylate), and Polystyrene. *J. Phys. Chem.* **1970**, *74*, 632−638.
(43) Berry, J. D.; Neeson, M. J.; Dagastine, R. R.; Chan, D. Y. C.; Tabor, R. F. Measurement of Surface and Interfacial Tension Using Pendant Drop Tensiometry. *J. Colloid Interface Sci.* **2015**, *454*, 226−237.

DOI: 10.1021/acs.langmuir.8b02071
Langmuir 2018, 34, 14012−14021

(44) Chakraborty, T.; Chakraborty, I.; Ghosh, S. The Methods of Determination of Critical Micellar Concentrations of the Amphiphilic Systems in Aqueous Medium. *Arab. J. Chem.* **2011**, *4*, 265−270.
(45) Crocker, J. C.; Grier, D. G. Methods of Digital Video Microscopy for Colloidal Studies. *J. Colloid Interface Sci.* **1996**, *179*, 298−310.
(46) Mohraz, A.; Solomon, M. J. Direct Visualization of Colloidal Rod Assembly by Confocal Microscopy. *Langmuir* **2005**, *21*, 5298−5306.
(47) Baroud, C. N.; Gallaire, F.; Dangla, R. Dynamics of Microfluidic Droplets. *Lab Chip* **2010**, *10*, 2032−2045.
(48) Driessen, T.; Jeurissen, R.; Wijshoff, H.; Toschi, F.; Lohse, D. Stability of Viscous Long Liquid Filaments. *Phys. Fluids* **2013**, *25*, 062109.
(49) Li, Z.; Lee, K.; Kepkey, P. E.; Mikkelsen, O.; Pottsmith, C. Monitoring Dispersed Oil Droplet Size Distribution at the Gulf of Mexico Deepwater Horizon Spill Site. *Int. Oil Spill Conf. Proc.* **2011**, *2011*, abs377.
(50) Harris, J. M.; Martin, L. F. An in vitro Study of the Properties Influencing *Staphylococcus epidermidis* Adhesion to Prosthetic Vascular Graft Materials. *Ann. Surg.* **1987**, *206*, 612−620.
(51) Liu, Y.; Shen, L. From Langmuir Kinetics to First- and Second-Order Rate Equations for Adsorption. *Langmuir* **2008**, *24*, 11625−11630.
(52) Al-Rashed, S. M.; Al-Gaid, A. A. Kinetic and Thermodynamic Studies on the Adsorption Behavior of Rhodamine B Dye on Duolite C-20 Resin. *J. Saudi Chem. Soc.* **2012**, *16*, 209−215.
(53) Kankare, J.; Vinokurov, I. A. Kinetics of Langmuirian Adsorption onto Planar, Spherical, and Cylindrical Surfaces. *Langmuir* **1999**, *15*, 5591−5599.
(54) Dasgupta, S.; Katava, M.; Faraj, M.; Auth, T.; Gompper, G. Capillary Assembly of Microscale Ellipsoidal, Cuboidal, and Spherical Particles at Interfaces. *Langmuir* **2014**, *30*, 11873−11882.
(55) Coertjens, S.; De Dier, R.; Moldenaers, P.; Isa, L.; Vermant, J. Adsorption of Ellipsoidal Particles at Liquid-Liquid Interfaces. *Langmuir* **2017**, *33*, 2689−2697.
(56) Marshall, K. C.; Cruickshank, R. H. Cell Surface Hydrophobicity and the Orientation of Certain Bacteria at Interfaces. *Arch. Mikrobiol.* **1973**, *91*, 29−40.
(57) Levine, S.; Bowen, B. D.; Partridge, S. J. Stabilization of Emulsions by Fine Particles I. Partitioning of Particles Between Continuous Phase and Oil/Water Interface. *Colloids Surf.* **1989**, *38*, 325−343.
(58) Abdel-Fattah, A. I.; El-Genk, M. S. Sorption of Hydrophobic, Negatively Charged Microspheres onto a Stagnant Air/Water Interface. *J. Colloid Interface Sci.* **1998**, *202*, 417−429.
(59) Loudet, J. C.; Alsayed, A. M.; Zhang, J.; Yodh, A. G. Capillary Interactions Between Anisotropic Colloidal Particles. *Phys. Rev. Lett.* **2005**, *94*, 018301.
(60) Madivala, B.; Fransaer, J.; Vermant, J. Self-Assembly and Rheology of Ellipsoidal Particles at Interfaces. *Langmuir* **2009**, *25*, 2718−2728.
(61) Lewandowski, E. P.; Searson, P. C.; Stebe, K. J. Orientation of a Nanocylinder at a Fluid Interface. *J. Phys. Chem. B* **2006**, *110*, 4283−4290.
(62) Adams, D. J.; Adams, S.; Melrose, J.; Weaver, A. C. Influence of Particle Surface Roughness on the Behaviour of Janus Particles at Interfaces. *Colloids Surf. A* **2008**, *317*, 360−365.
(63) San-Miguel, A.; Behrens, S. H. Influence of Nanoscale Particle Roughness on the Stability of Pickering Emulsions. *Langmuir* **2012**, *28*, 12038−12043.
(64) Isa, L.; Lucas, F.; Wepf, R.; Reimhult, E. Measuring Single-Nanoparticle Wetting Properties by Freeze-Fracture Shadow-Casting Cryo-Scanning Electron Microscopy. *Nat. Commun.* **2011**, *2*, 438.
(65) Park, B. J.; Lee, D. Equilibrium Orientation of Nonspherical Janus Particles at Fluid-Fluid Interfaces. *ACS Nano* **2012**, *6*, 782−790.
(66) Park, B. J.; Lee, D. Configuration of nonspherical amphiphilic particles at a fluid-fluid interface. *Soft Matter* **2012**, *8*, 7690−7698.
(67) Isa, L.; Samudrala, N.; Dufresne, E. R. Adsorption of Sub-Micron Amphiphilic Dumbbells to Fluid Interfaces. *Langmuir* **2014**, *30*, 5057−5063.
(68) Zanini, M.; Marschelke, C.; Anachkov, S. E.; Marini, E.; Synytska, A.; Isa, L. Universal Emulsion Stabilization from the Arrested Adsorption of Rough Particles at Liquid-Liquid Interfaces. *Nat. Commun.* **2017**, *8*, 15701.
(69) van der Vegt, W.; Norde, W.; van der Mei, H. C.; Busscher, H. J. Kinetics of Interfacial Tension Changes during Protein Adsorption from Sessile Droplets on FEP-Teflon. *J. Colloid Interface Sci.* **1996**, *179*, 57−65.
(70) Nave, S.; Eastoe, J.; Heenan, R. K.; Steytler, D.; Grillo, I. What Is So Special about Aerosol-OT? 2. Microemulsion Systems. *Langmuir* **2000**, *16*, 8741−8748.
(71) Dey, J.; Bhattacharjee, J.; Hassan, P. A.; Aswal, V. K.; Das, S.; Ismail, K. Micellar Shape Driven Counterion Binding. Small-Angle Neutron Scattering Study of AOT Micelle. *Langmuir* **2010**, *26*, 15802−15806.
(72) Nakahara, H.; Shibata, O.; Moroi, Y. Examination of Surface Adsorption of Cetyltrimethylammonium Bromide and Sodium Dodecyl Sulfate. *J. Phys. Chem. B* **2011**, *115*, 9077−9086.
(73) Hildebrandt, E.; Sommerling, J.-H.; Guthausen, G.; Zick, K.; Stürmer, J.; Nirschl, H.; Leneweit, G. Phospholipid Adsorption at Oil in Water Versus Water in Oil Interfaces: Implications for Interfacial Densities and Bulk Solubilities. *Colloids Surf. A* **2016**, *505*, 56−63.
(74) Nave, S.; Eastoe, J.; Penfold, J. What Is So Special about Aerosol-OT? 1. Aqueous Systems. *Langmuir* **2000**, *16*, 8733−8740.
(75) Bookstaver, M.; Bose, A.; Tripathi, A. Interaction of Alcanivorax borkumensis with a Surfactant Decorated Oil-Water Interface. *Langmuir* **2015**, *31*, 5875−5881.
(76) McEldowney, S.; Fletcher, M. Variability of the Influence of Physicochemical Factors Affecting Bacterial Adhesion to Polystyrene Substrata. *Appl. Environ. Microbiol.* **1986**, *52*, 460−465.
(77) Thaveesri, J.; Daffonchio, D.; Liessens, B.; Vandermeren, P.; Verstraete, W. Granulation and Sludge Bed Stability in Upflow Anaerobic Sludge Bed Reactors in Relation to Surface Thermodynamics. *Appl. Environ. Microbiol.* **1995**, *61*, 3681−3686.
(78) Zhang, X.; Zhang, Q.; Yan, T.; Jiang, Z.; Zhang, X.; Zuo, Y. Y. Quantitatively Predicting Bacterial Adhesion Using Surface Free Energy Determined with a Spectrophotometric Method. *Environ. Sci. Technol.* **2015**, *49*, 6164−6171.
(79) Singh, O. G.; Ismail, K. Effect of Sodium Chloride on the Aggregation, Adsorption and Counterion Binding Behavior of Mixtures of Sodium Dioctylsulfosuccinate and Sodium Dodecylsulfate in Water. *Colloids Surf. A* **2012**, *414*, 209−215.
(80) Abbasi, A.; Bothun, G. D.; Bose, A. Attachment of *Alcanivorax borkumensis* to Hexadecane-In-Artificial Sea Water Emulsion Droplets. *Langmuir* **2018**, *34*, 5352−5357.
(81) Zenati, B.; Chebbi, A.; Badis, A.; Eddouaouda, K.; Boutoumi, H.; El Hattab, M.; Hentati, D.; Chelbi, M.; Sayadi, S.; Chamkha, M.; Franzetti, A. A Non-Toxic Microbial Surfactant from Marinobacter hydrocarbonoclasticus SdK644 for Crude Oil Solubilization Enhancement. *Exotoxicol. Environ. Saf.* **2018**, *154*, 100−107.
(82) Rusconi, R.; Stocker, R. Microbes in Flow. *Curr. Opin. Microbiol.* **2015**, *25*, 1−8.
(83) Conrad, J. C.; Poling-Skutvik, R. Confined Flow: Consequences and Implications for Bacteria and Biofilms. *Annu. Rev. Chem. Biomol. Eng.* **2018**, *9*, 175−200.
(84) Godfrin, M. P.; Sihlabela, M.; Bose, A.; Tripathi, A. Behavior of Marine Bacteria in Clean Environment and Oil Spill Conditions. *Langmuir* **2018**, *34*, 9047−9053.
(85) Kaminski, T. S.; Scheler, O.; Garstecki, P. Droplet Microfluidics for Microbiology: Techniques, Applications and Challenges. *Lab Chip* **2016**, *16*, 2168−2187.
(86) Cydzik-Kwiatkowska, A.; Zielińska, M. Bacterial Communities in Full-Scale Wastewater Treatment Systems. *World J. Microbiol. Biotechnol.* **2016**, *32*, 66.

DOI: 10.1021/acs.langmuir.8b02071
Langmuir 2018, 34, 14012−14021